17th World Conference on Earthquake Engineering, 17WCEE
Sendai, Japan - September 13th to 18th 2020

EXPERIMENTAL STUDY OF SELF-CENTERING CONCRETE SHEAR WALLS WITH EXTERNAL FRICTION DISSIPATERS

Y. Liu[(1)], W. Zhou[(2)]

[(1)] *Ph.D. Student, Harbin Institute of Technology, P.R. China, liuyanghit2012@stu.hit.edu.cn*
[(2)] *Professor, Harbin Institute of Technology, P.R. China, zhouwei-hit@163.com*

Abstract

Post-earthquake resilience of engineering structures is an important research area of sustainable earthquake engineering in recent years. As an important component of earthquake resilient structural system, self-centering shear wall system are drawing more attention of many researchers [1-2]. Restoration and collapse control are realized with the constraint at the base released and the wall panels post-tensioned by unbonded prestressing tendons, which can reduce damage level and even eliminate residual drift owing to the gap-opening mechanism. However, the fracture of prestressing tendons and internal dissipaters was observed in previous experimental studies, which results in sudden increase of structural response [3-4]. Self-centering structural system still suffers from the lack of redundancy and robustness. In this study, the seismic performance of 10 ordinary self-centering concrete shear walls were studied first under quasi-static test, including the stiffness, deterioration, dissipating and restoration capacity. Then a new type of external friction dissipater was designed, and 19 specimens were tested. Steel, brass and carbon fiber sheets were used as the friction plates, and all the specimens showed perfect rigid-plastic performance. Finally, in order to build multiple defense of collapse, the friction dissipaters were arranged at different position at the bottom rocking interface of the self-centering wall. 3 specimens were tested under cyclic loading, and a preliminary analysis of the hierarchical activation manner of different set of dissipaters was presented in this part of research.

Keywords: experimental study; self-centering concrete shear wall; external friction dissipater

1. Introduction

In recent years, post-earthquake resilience is getting more and more attention from the researchers from all over the world. As an effective way to achieve restoration, self-centering plays an important role to reduce damage and economy loss. To investigate the seismic performance of the self-centering walls, 10 ordinary concrete shear walls were tested first under quasi-static cyclic horizontal loading, including 3 rocking walls without axial loading, 1 cast-in-site wall and 6 self-centering walls with additional axial loading. Then 19 external isolated friction dissipaters were designed and tested. Finally, external friction dissipaters were introduced in the self-centering walls, and in this part, 3 walls with external friction dissipaters were tested under quasi static cyclic horizontal loading without additional axial loading.

2. Cyclic test of ordinary self-centering concrete shear walls

2.1 Specimen design

To evaluate the basic performance, several parameters were considered, including the additional axial load, prestressing load, and dissipating. Three 2/3 scale rocking walls were tested without axial loading, and seven full-scale concrete shear walls were tested under constant axial loading, including six self-centering walls with dissipating steel bars and one cast-in-site wall as comparison. Details of the parameters are listed in Table 1.

N series walls were rocking walls without dissipating bars, and the prestressing load was increasing from NL0 to NH0. B series walls were self-centering walls, and were designed based on the method proposed by Smith [5], that to achieve restoration, the self-centering force (including the axial load and prestressing load)

must be able to compress the dissipating devices (like steel bars) from tensile yielding to compressive yielding. Given this idea, B series walls were categorized to three classes: BM1-13 and BL2-15 represented low self-centering ability, since the axial load and prestressing load were low, but the area of dissipating bars was large; Similarly, BM2-13-1 and BM2-13-2 represented the middle self-centering ability, and BH2-11-1 and BH2-11-2 represented the highest self-centering ability. And also, the spacing between the dissipating bars was changed for BM2-13-2 and BH2-11-2, to evaluate the best arrangement of the dissipating bars.

Table 1 – List of the test wall specimens

Specimen No.	Number of tendons	Initial tendon stress (MPa)	Position of the tendons (to centroid line, mm)	Additional axial load (kN)	Dissipating bars	Position of the dissipating bars (to centroid line, mm)
NL0	2	558	±150	–	–	–
NM0	3	558	0, ±150	–	–	–
NH0	3	744	0, ±150	–	–	–
BM1-13	3	744	0, ±150	319.7	8Φ13	±45, ±105
BM2-13-1	3	744	0, ±150	639.4	8Φ13	±45, ±105
BL2-15	2	744	±150	639.4	8Φ15	±45, ±105
BH2-11-1	3	1023	0, ±150	639.4	8Φ11	±45, ±105
BM2-13-2	3	744	0, ±150	639.4	8Φ13	±75, ±225
BH2-11-2	3	1023	0, ±150	639.4	8Φ11	±105, ±315
EW	–	–	–	952	–	–

The cross section of N series walls was 1000mm*140mm, and the height (vertical distance from the horizontal loading force to the bottom of the wall) was 2.0m; the cross section of B series walls and EW was 1500mm*160mm, and the height was 3.4m. Prestressing strands were placed in the metal corrugated flat ducts embedded in the wall specimens, and Φ18 bars were used as the dissipating bars in B series walls, with two ends anchored in the wall and foundation beam. Within the bottom 300mm height of the wall, dissipating bars were wrapped by PVC ducts to be unbonded, and manufactured to different diameters in this area. Details of the reinforcement is illustrated in Fig. 1. The distributed bars were Φ8@150mm in both vertical and horizontal direction for all the specimens and are omitted in Fig. 1 for clarity.

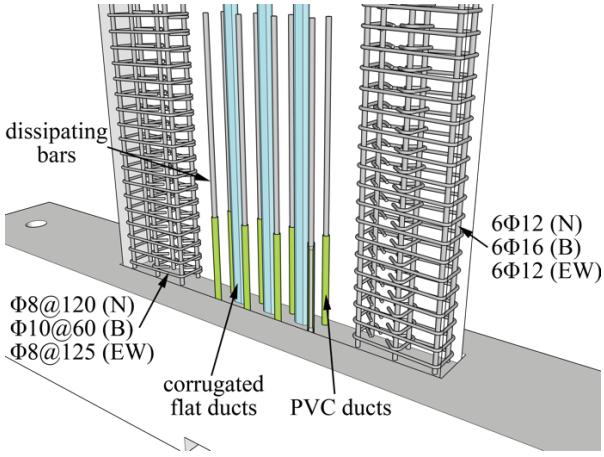

Fig. 1 – Wall reinforcement

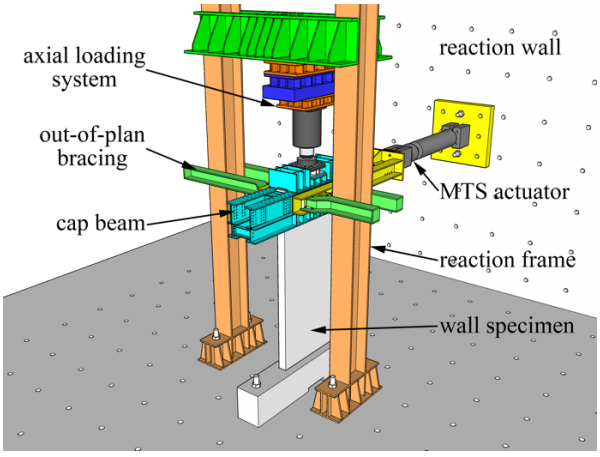

Fig. 2 – Test setup

2.2 Properties of materials

The design grade of concrete was C40, and the average cubic compressive strength was 47.8 MPa (tested from 150mm*150mm*150mm cubes). 1*7 wire grade 1860 prestressing strands were used as the post-tensioned tendon. Properties of the steel bars and tendon are listed in Table 2 and Table 3.

Table 2 – Properties of the steel bars

Grade	HPB300		HRB400		
Diameter (mm)	Φ8	Φ10	Φ12	Φ16	Φ18
Yield strength (MPa)	367.8	351.1	478.5	446.4	466.5
Ultimate strength (MPa)	538.3	512.0	669.3	648.9	656.9

Table 3 – Properties of the tendon

Diameter (mm)	Yield strength (MPa)	Ultimate Strength (MPa)	Elastic modulus (MPa)
Φ15.2	1679.5	1928.1	1.966×10^5

2.3 Test setup, instrumentation and loading protocol

Fig. 2 illustrates the test setup. The cyclic horizontal force was provided by an MTS actuator, and the axial load was applied by a hydraulic jack, which could slide within the slide rail in the direction of the horizontal force to ensure the axial load always be vertical. The hydraulic jack was controlled by an electric servo-controlled system to produce constant axial load. For N series walls, the axial load was not applied during test.

Two different loading protocol were adopted, as shown in Fig. 3 and Fig.4. Loading of N series walls was totally displacement-controlled, with an increment of 0.25% drift between different displacement level until 3.0% drift and repeated twice in every drift level. For B series walls and EW, loading was force-controlled first, then displacement-controlled until 3.0% drift after yielding and repeated three times in every drift level. Also, the increment between different drift level was increasing [6] to avoid excess loading cycles. Fig. 5 illustrates the instrumentation details. Three linear voltage displacement transducers (LVDTs) were mounted to monitor the horizontal displacement at the top, middle height of the wall, and the foundation beam. Four LVDTs were arranged vertically at the bottom rocking interface to measure the gap opening. Beside this, forces were measured by load cells embedded in the MTS actuator and the vertical hydraulic jack.

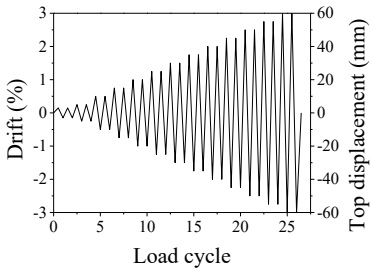

Fig. 3 – Loading protocol of N series walls

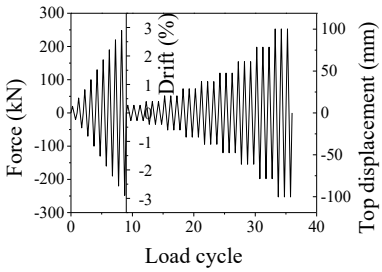

Fig. 4 – Loading protocol of B series walls and EW

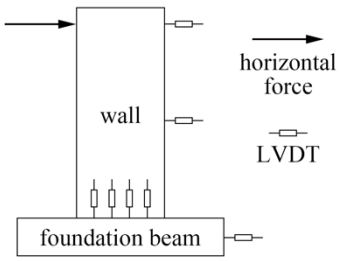

Fig. 5 – Instrumentation

2.4 Test results and analysis

All the specimens exhibited minor damage and little residual drift except EW. Damage was limited to cover concrete spalling in very small range (within bottom 400mm height), and the stirrups in boundary elements

worked well as shown in Fig. 6 (b). However, EW underwent severe damage including buckling of longitudinal bars and core concrete crush. Hysteretic curves of NM0, BM2-13-2 and EW are showed in Fig. 7.

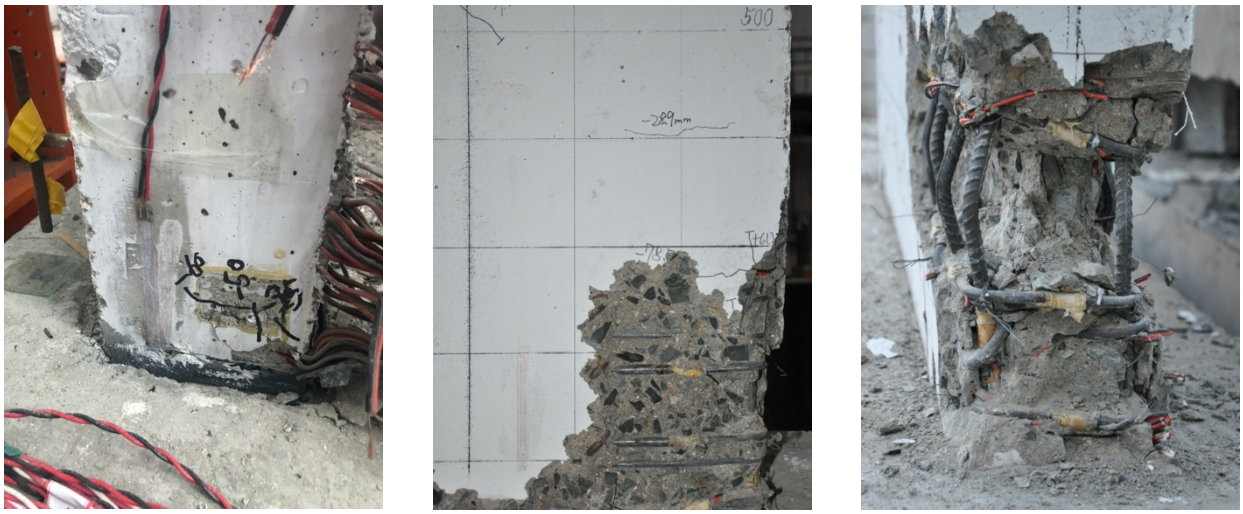

(a) NM0 (b) BM2-13-2 (c) EW

Fig. 6 – Damage after tests

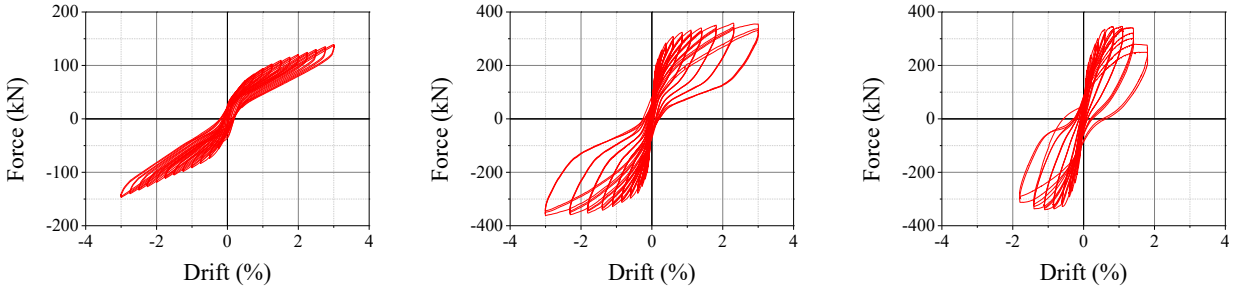

(a) NM0 (b) BM2-13-2 (c) EW

Fig. 7 – Hysteretic curves

Envelop curves and residual drift of all the test walls are showed in Fig. 8 and Fig. 9, respectively. N series walls exhibited very poor hysteretic performance, as observed by the narrow loops. As shown in Fig. 8, specimens got higher resistance and stiffness for increasing prestressing load, but also resulted in the fracture of the tendon in NH0.

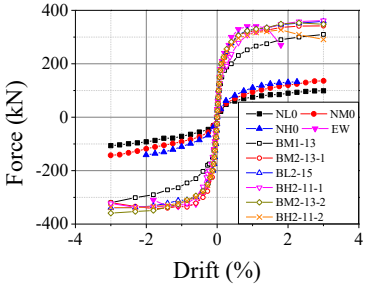

Fig. 8 – Envelop curves

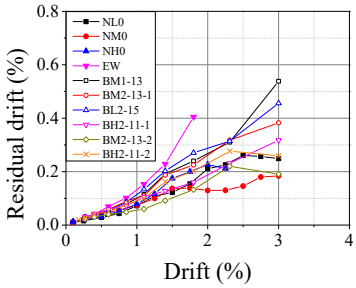

Fig. 9 – Residual drift

For B series walls, the resistance, stiffness and hysteretic performance were better by introducing dissipating bars, but also result in larger residual drift. Since the dissipating bar spacing of BH2-11-2 was the largest one, three dissipating bars and some wires of the prestressing strands fractured, resulting in the deterioration of the horizontal resistance. Specimen EW showed the highest initial stiffness, but the horizontal resistance dropped more rapidly to less than 80% of the ultimate at 1.8% drift and underwent the highest

residual drift. Several studies have defined 1.0% residual drift as the permissible value for seismic design in concrete structures [7, 8], and the residual drift of all the test specimens was far below this limit except EW, indicating perfect self-centering ability.

3. Cyclic test of isolated friction dissipaters

3.1 Specimen design

During horizontal loading of the self-centering wall, the wall will rock up and down at the bottom. Based on the gap opening measured in previous section, 19 friction dissipaters were designed and tested under cyclic loading.

As shown in Fig. 10, the dissipater consisted of three steel plates and two friction sheets and was pre-tensioned to stack together by bolts. Top steel plate, bottom steel plate and the friction sheets will move synchronously, and slide in the long slots on the main steel plate during test. Pre-tensioned force was controlled by the torque applied to the bolts, and the bolts were load twice to give a balanced pre-tension load. First to 50% of the target torque, and diagonally, then to 100% of the target torque. Several parameters were considered, including the type of the friction sheets, number of the slots on the main steel plate, and the pre-tension force provided by bolts. Steel, brass and carbon/carbon (C/C) were used as the friction sheets. There were one, two, three slots on the main steel plate for three different types, and two bolts were pre-tensioned for every slot.

Table 4 summarizes all the parameters of B series test specimens for example. As for the specimen No., the first capital letter represented different friction sheet type, A for steel, B for brass, and C for C/C. The second number represented the number of slots on the main steel plate, and the final number represented the torque of every bolt. The configuration of C series dissipaters was identical with B series dissipaters except B0-2-250 and B00-2-250, only the friction sheets were replaced by C/C materials. Another dissipater A-2-250 using steel brass sheets was added as comparison.

Table 4 – List of B series test dissipaters

Specimen No.	No. of the slots	No. of the bolts	Friction sheet type	Thickness of the friction sheets (mm)	Torque of every bolt (N*m)	Total torque (N*m)
B-1-300	1	2	Brass	2	300	1000
B-2-150	2	4		2	150	600
B-2-200	2	4		2	200	800
B-2-250	2	4		2	250	1000
B-2-300	2	4		2	300	1200
B0-2-250	2	4		0.5	250	1000
B00-2-250	2	4		0.5*4	250	1000
B-3-100	3	6		2	100	600
B-3-150	3	6		2	150	900
B-3-200	3	6		2	200	1200

Note: The thickness of all the friction sheets was 2.0mm, but for B0-2-250, the thickness of the friction sheet was 0.5mm, and for B00-2-250, four 0.5mm-thickness plates were stacked together as one 2mm-thickness friction sheet.

3.2 Test setup, instrumentations and loading protocol

The test setup is illustrated in Fig. 11. The rigid concrete circle beam provided a self-balanced system. Main plate was fixed, and the bottom steel was connected to a hydraulic jack and loaded cyclically. Loading protocol was displacement-controlled, as shown in Fig.12. Target displacement level was 20mm, 40mm and 60mm, and repeated twice for every level. Force was monitored by a connected load cell, and two LVDTs were used to measure the displacement of the top steel plate and the bottom steel plate.

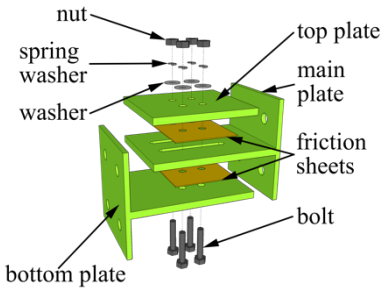

Fig. 10 – Assembling view of the dissipater (two-slot dissipater for example)

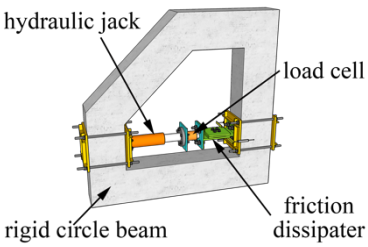

Fig. 11 – Test setup

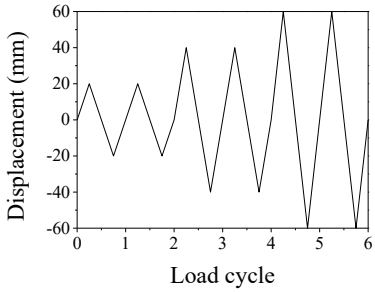

Fig. 12 – Loading protocol

3.3 Test results and analysis

The lateral resistance versus displacement curve of B-2-250 is illustrated in Fig. 13. Most of the hysteretic curves were rectangular and without resistance deterioration. However, for specimen A-2-250 and B00-2-250, the resistance increased for increasing displacement level. The friction sheets deformed badly and crushed into the slots, as shown in Fig. 14 (a), which provided additional dowel force except friction. Although the resistance was high, it was based on the large damage of the friction sheets and unstable dissipating. Also, the friction sheets of B0-2-250 was broken after test as shown in Fig. 14 (b). 0.5mm-thickness brass sheets were too thin to remain integrity, and significant deterioration could be observed from the hysteretic curve.

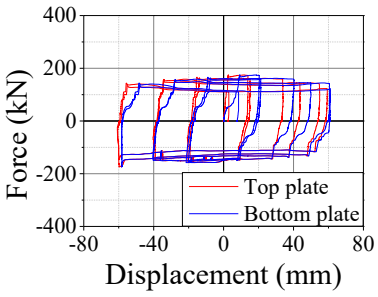

Fig. 13 – Hysteretic curve (B-2-250)

(a) A-2-250

(b) B0-2-250

Fig. 14 – Broken friction sheets

To evaluate the performance of the friction dissipaters, the equivalent coefficient of friction β was calibrated, which was the ratio of the force of friction f to the pre-tension force from the bolts P:

$$\beta = \frac{f}{P} \tag{1}$$

Since,

$$f = \mu F_N \tag{2}$$

Where μ is the coefficient of friction, and F_N is the normal force. Torque is defined by [9]

$$T = kPd \tag{3}$$

Where P was the pre-tension force from bolts, d was the diameter of the bolt, and k was 0.12 provided by manufacturer. However, the normal force is not identical with the pre-tension force from bolts, then

$$F_N = \alpha P \tag{4}$$

Where α was a coefficient, thus from Eq. (1) to Eq. (4), the equivalent coefficient of friction β is

$$\beta = \frac{f}{P} = \mu\alpha = \frac{fkd}{T} \tag{5}$$

Stable slip process (every second loop of the 20mm cycle) was chose to calculate the equivalent coefficient of friction β. Force of friction was calculated as the average absolute value of both positive and negative direction, and the results are listed in Table 5. β of A-2-250, B00-2-250 and B0-2-250 was not calculated, because these specimens could not provide stable hysteretic performance.

Table 5 – Calculation of the equivalent coefficient of friction β

Specimen No.	β	Average β	Specimen No.	β	Average β
B-1-300	0.172	0.172	C-1-300	0.084	0.084
B-2-150	0.488	0.412	C-2-150	0.167	0.195
B-2-200	0.395		C-2-200	0.204	
B-2-250	0.380		C-2-250	0.209	
B-2-300	0.383		C-2-300	0.200	
B-3-100	0.253	0.312	C-3-100	0.111	0.120
B-3-150	0.316		C-3-150	0.099	
B-3-200	0.366		C-3-200	0.151	

The contact area on the main plate decreased with increasing number of slots, thus dissipaters with two slots on the main plate underwent the highest equivalent coefficient of friction, as listed in Table 5. β of the dissipaters using C/C friction sheets was lower, that might because this material was usually used in more severe situations, like the brake disc of the aircrafts of sport cars, which suffered a low coefficient of friction at temperature below 450℃ [10]. Thus, in the following section, dissipaters with two slots and brass friction sheets were introduced to the self-centering walls.

4. Cyclic test of self-centering walls with external friction dissipaters

4.1 Specimen design

Three walls with external friction dissipaters were designed and tested. The dimension and reinforcement were identical with N series walls, but external friction dissipaters were installed at the bottom rocking interface to provide additional dissipating, as shown in Fig.15 and Fig. 16. Total torque of all the dissipaters was 240N*m, and details of the parameters are listed in Table 6. The only difference between NL0 and FL0-E1, NM0 and FM0-E2 was the added dissipaters. Another specimen FM0-E1 was designed to investigate the influence of the dissipater arrangement.

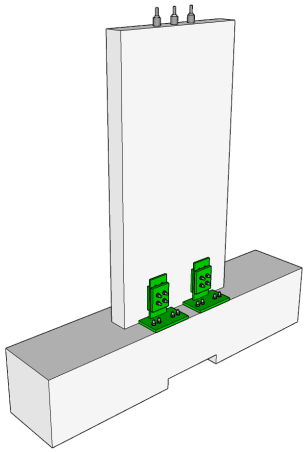

Fig. 15 – Overview of the wall with external friction dissipaters (FM0-E2)

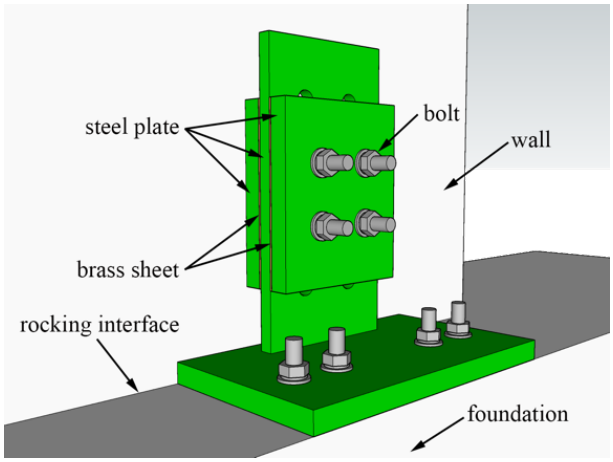

Fig. 16 – External friction dissipater design

Table 6 – List of the test walls

Specimen No.	Number of tendons	Initial tendon stress (MPa)	Position of the tendons (to centroid line, mm)	Additional axial load (kN)	Number of the friction dissipaters	Position of the dissipaters (to centroid line, mm)	Total torque of all the dissipaters (N*m)
FL0-E1	2	0.3	±150	–	6	0, ±215	240
FM0-E2	3	0.3	0, ±150	–	4	±215	240
FM0-E1	3	0.3	0, ±150	–	6	0, ±215	240

4.2 Test setup, instrumentations and loading protocol

The test setup, instrumentations and loading protocol were identical with the cyclic test of the N series walls.

4.3 Test results and analysis

Hysteretic curve of FM0-E1 is illustrated in Fig. 17. Envelop curves and residual drift of all the test walls are illustrated in Fig. 18 and Fig. 19, and the results of NL0 and NM0 are added as comparison.

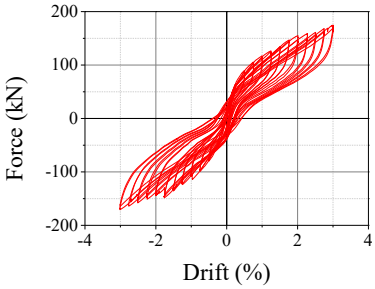

Fig. 17 – Hysteretic curve (FM0-E1)

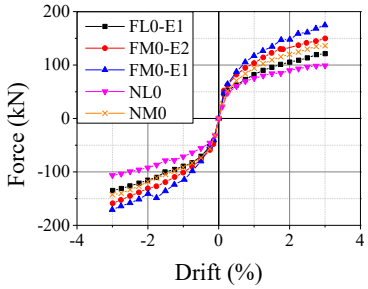

Fig. 18 – Envelop curves

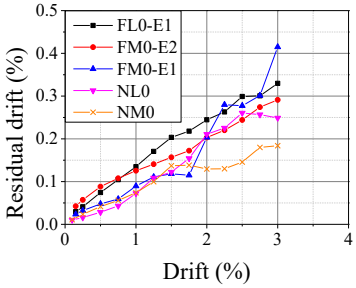

Fig. 19 – Residual drift

By introducing external friction dissipaters, F series walls exhibited better hysteretic performance than N series walls, and residual drift increased slightly but still far below 1.0%. The initial stiffness was almost the same for F series walls and N series walls, but the stiffness after yielding of F series walls was higher. FM0-

E2 had fatter hysteretic loop, higher stiffness than FM0-E1, though the total pre-tension force were the same. Tendons were observed fractured in FM0-E1, but the resistance still increased in higher drift levels.

4.4 Hierarchical activation manner

Friction dissipaters have stable dissipating ability without hardening and deterioration, and larger deformation capacity than mild steel bars. Since the friction dissipaters were placed externally, they are easy to be replaced after earthquake, and damage was usually limited to the friction sheets. Many researchers have conducted studies of the friction dissipaters and structural system with friction dissipaters [11-13], which showed perfect self-centering performance.

However, three dissipating bars of BH2-11-2 fractured during cyclic test, resulting the deterioration of lateral resistance. In order to increase the redundancy and robustness, a hierarchical activation manner could be proposed by combining the internal bar dissipating and external friction dissipating. As illustrated in Fig. 18, there was almost no difference with the initial stiffness by introducing friction dissipaters, initial stiffness could be increased with added internal dissipating bars, and in ultimate state, very large horizontal drift for example, the external friction dissipaters will still work after the dissipating bars fractured, which could build multiple fuses to prevent collapse. This could be verified in experiments or simulation in the future.

5. Conclusion

The following conclusions could be drawn from the experiments and analysis conducted in this study:

1) The rocking wall and self-centering wall specimens showed perfect self-centering ability and minor damage, but the fracture of dissipating bars and prestressing strands, and resistance deterioration were observed, indicating insufficient redundancy and robustness.

2) Friction dissipater could provide stable dissipating performance. Self-centering walls with external friction dissipaters showed higher stiffness and resistance, and the residual drift still far below limit.

3) A method to improve the redundancy and robustness was proposed by combining internal bar dissipating and external friction dissipating, which could be verified in the following experiment or simulation.

6. Acknowledgements

This study was sponsored by the National Natural Science Foundation of China (NSFC) (No. 51778186) and China Scholarship Council (CSC) (No. 201906120286).

7. References

[1] Wu H, Zhou Y, Liu W (2019): Collapse fragility analysis of self-centering precast concrete walls with different post-tensioning and energy dissipation designs. *Bulletin of Earthquake Engineering*, 17(6), 3593-3613.

[2] Gu A, Zhou Y, Xiao Y, et al (2019): Experimental study and parameter analysis on the seismic performance of self-centering hybrid reinforced concrete shear walls. *Soil Dynamics and Earthquake Engineering*, 116, 409-420.

[3] Yamashita, R, Sanders DH (2009): Seismic Performance of Precast Unbonded Prestressed Concrete Columns. *ACI Structural Journal*, 106(6), 812-830.

[4] Schoettler MJ, Belleri A, Zhang D, et al (2009): Preliminary results of the shake-table testing for the development of a diaphragm seismic design methodology. *PCI Journal*, 54(1), 100-124.

[5] Smith BJ (2012): *Design, analysis, and experimental evaluation of hybrid precast concrete shear walls for seismic regions*. University of Notre Dame.

[6] Applied Technology Council, Mid-America Earthquake Center, Multidisciplinary Center for Earthquake Engineering Research (US), et al (2007): *Interim Testing Protocols for Determining the Seismic Performance Characteristics of Structural and Nonstructural Components*. Federal Emergency Management Agency.

[7] Kawashima K, MacRae GA, Hoshikuma J, et al (1999): Residual displacement response spectrum. *Journal of Structural Engineering*, 124(5), 523-530.

[8] Sakai J, Unjoh S (2007): Shake table experiment on circular reinforced concrete bridge column under multidirectional seismic excitation. *Structural Engineering Research Frontiers*, 1-12.

[9] Chinese Ministry of Housing and Urban Rural Development (2011): *Technical specification for high strength bolt connections of steel structures, JGJ 82-2011*. China Architecture and Building Press. (in Chinese).

[10] Stadler Z, Krnel K, Kosmac T (2007): Friction behavior of sintered metallic brake pads on a C/C–SiC composite brake disc. *Journal of the European Ceramic Society*, 27(2-3), 1411-1417.

[11] Loo WY, Quenneville P, Chouw N (2012): A numerical study of the seismic behaviour of timber shear walls with slip-friction connectors. *Engineering Structures*, 34, 233-243.

[12] Loo WY, Quenneville P, Chouw N (2014): A new type of symmetric slip-friction connector. *Journal of Constructional Steel Research*, 94, 11-22.

[13] Guo T, Wang L, Xu Z, et al (2018): Experimental and numerical investigation of jointed self-centering concrete walls with friction connectors. *Engineering Structures*, 161, 192-206.

